Liquid Crystals
Publication details, including instructions for authors and subscription information:
http://www.informaworld.com/smpp/title~content=t713926090

Synthesis and characterization of a chiral antiferroelectric series with new SmC A*-L transition

V. Faye; J. C. Rouillon; H. T. Nguyen; L. Detre; V. Laux; N. Isaert

Online publication date: 06 August 2010

To cite this Article Faye, V. , Rouillon, J. C. , Nguyen, H. T. , Detre, L. , Laux, V. and Isaert, N.(1998) 'Synthesis and characterization of a chiral antiferroelectric series with new SmC A*-L transition', Liquid Crystals, 24: 5, 747 — 758
To link to this Article: DOI: 10.1080/026782998206876
URL: http://dx.doi.org/10.1080/026782998206876

LIQUID CRYSTALS, 1998, VOL. 24, NO. 5, 747–758

Synthesis and characterization of a chiral antiferroelectric series with new SmC_A^*–L transition

by V. FAYE, J. C. ROUILLON, H. T. NGUYEN*
Centre de Recherche Paul Pascal, Av. A. Schweitzer, 33600 Pessac, France

L. DÉTRÉ, V. LAUX and N. ISAERT
Laboratoire de Dynamique et Structure des Matériaux Moléculaires,
Université de Lille I, 59 655 Villeneuve d'Ascq, France

(*Received 1 August 1997; in final form 24 November 1997; accepted 11 December 1997*)

Two new chiral series with a tolane core: (*S*) 4-(1-methylheptyloxycarbonyl)phenyl (series IB) and (*S*) 4-(1-ethylheptyloxycarbonyl)phenyl (series IC) 4-alkanoyloxytolane-4′-carboxylates have been synthesized and characterized. All the compounds are mesomorphic, and most of them display the antiferroelectric SmC_A^* phase. The mesomorphic properties have been analysed by optical microscopy, DSC, helical pitch and electro-optical measurements and X-ray diffraction study. Series IB exhibits a very rich polymesomorphism with SmC_α^*, SmC*, SmC_{FI2}^*, SmC_{FI1}^* and SmC_A^* phases, like the previously reported series IA, [(*S*) 4-(1-methylheptyloxycarbonyl)phenyl 4-alkyloxytolane-4′-carboxylates]. Series IC is more interesting because it presents for the first time in antiferroelectric series the liquid-like phase (L phase) between the SmC_A^* and isotropic phases. Preliminary optical studies plead in favour of a helical short range structure for this new liquid-like L phase.

1. Introduction

A few years ago, chiral liquid crystals attracted new attention with the discovery of antiferroelectricity associated with the SmC_A^* phase [1]. Since then, research in this field has been aimed at improving the electro-optical properties and understanding the structures of other chiral smectic phases which are often associated with the SmC* phase, like SmC_{FI}^* and SmC_α^*. This goal could not be achieved without synthesizing new materials, necessary to understand better the relationship between chemical structure and liquid crystalline properties. By modifying stepwise the chemical structure of a given chiral compound, it is possible to gain information about the specific role of each chemical unit. Up to now, most antiferroelectric liquid crystals (AFLCs) have been designed following the model of 4-(1-methylheptyloxycarbonyl)phenyl 4′-octyloxybiphenyl-4-carboxylate (MHPOBC), which was the first compound to display the SmC_A^* phase [1]. Its formula is represented below. Most chemical modifications to the rigid core still lead to AFLC compounds [2–5], except for the use of a symmetrical group close to the chiral centre which favours the TGB_A phase [6, 7]. Only a few AFLC compounds bearing a different chiral chain have been reported so far. Substitution of hydrogen atoms of the CH_3 chiral branch by fluorine have been systematically investigated [8], and the effect of lengthening this short branch has also been studied [9, 10].

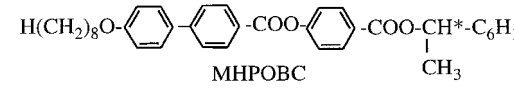

MHPOBC

In this paper, we report the synthesis and characterization of two series of low molar mass AFLC compounds: series IB and IC, represented below. Comparison of their mesomorphic behaviour may shed light upon the influence of the composition of the chiral moiety. Reference to series IA [(*S*) 4-(1-methylheptyloxycarbonyl)-phenyl 4-alkyloxytolane-4′-carboxylates] [4] is made for investigation of the role of the linkage between the non-chiral flexible chain length and the rigid core.

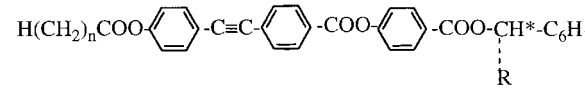

IB where R=CH_3

IC where R=C_2H_5

Over and above these structural considerations, series IC was found to display an unusual mesomorphic behaviour. A direct first-order transition between the

*Author for correspondence.

SmC_A^* and SmA phases was obtained for most members of this series. For the longest chain members, a thermal event has been detected in the isotropic range, which reminds one of those previously observed above a twist grain boundary (TGB) phase [11, 12]. The existence of such an 'isotropic' phase, also named L to distinguish it from the isotropic liquid, has never been detected for antiferroelectric materials previously. Also reported for the first time here is its textural characterization. Fluctuating twisting defects were detected by careful optical examination of a thin homeotropic drop.

2. Experimental

2.1. *Synthesis*

The synthetic route used (see the scheme) was the same for both series, except for the starting chiral alcohol. In series IA and IB, 2-(*S*)-octanol (Fluka) was used whereas 3-(*S*)-nonanol (Japan Energy Corporation) was used for series IC. Details of individual syntheses are given in § 5.

2.2. *Characterization*

2.2.1. *Chemical characterization*

The purity of all intermediate and final compounds was checked by thin layer chromatography (using Merck plastic sheets, silica gel 60). Their chemical structures were confirmed by ^1H NMR (Bruker AM200) and by Fourier transform infrared spectroscopy (Nicolet MX-1). The purity of final products was checked by normal phase HPLC using a Waters 600E system controller. Chromatography was carried out on silica gel (Waters Microporasil 10 mm particle size) using CH_2Cl_2 as eluent. Detection of the eluting products was achieved using a Waters 484 UV-VIS detector ($\lambda = 254$ nm). Each of the final products was found to have a purity exceeding

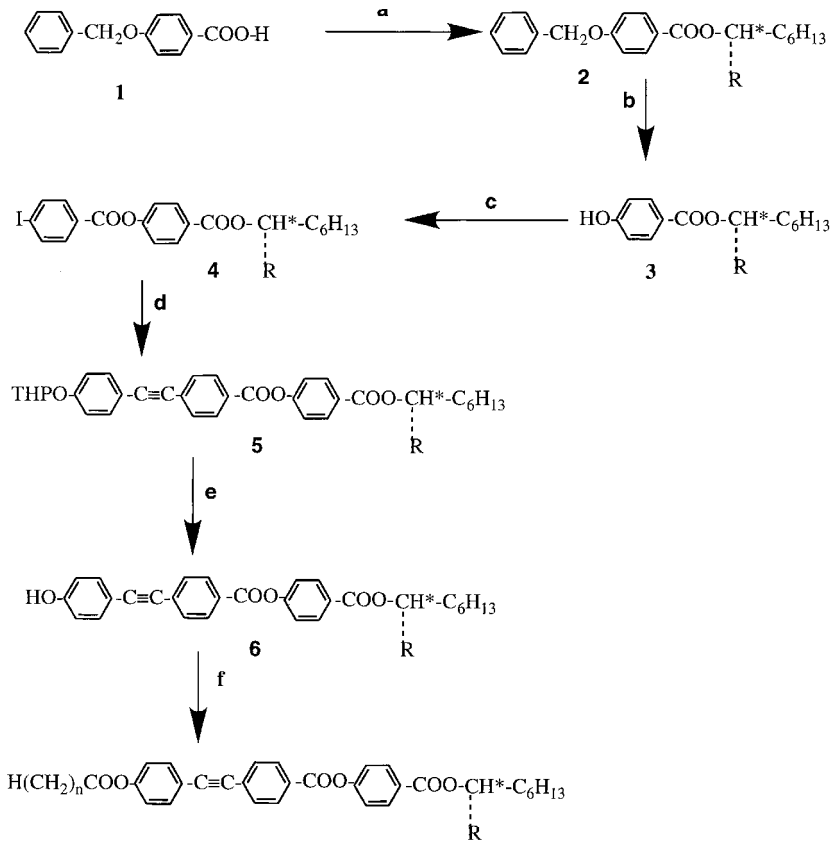

Scheme. Synthetic route for series IB and IC.

a: DCC, DMAP, CH_2Cl_2 ; b: H_2, Pd/C, AcOEt, EtOH (95%); c: I-Ph-COOH, DCC, DMAP, CH_2Cl_2; d: THPO-Ph-C≡C-H, $PdCl_2$, Cu(AcO)2; H_2O, TPP, iPr_2NH; e: PTSA, MeOH, THF; f: $H(CH_2)_n$-COOH, DCC, DMAP, CH_2Cl_2

99 per cent. The optical rotation was determined using a polarimeter (Perkin Elmer 341).

2.2.2. *Mesomorphic properties*

The thermal behaviour of the mesogens was investigated by differential scanning calorimetry (Perkin Elmer DSC7) and the first general phase identification was carried out by thermal optical microscopy, using a Zeiss Ortholux polarizing microscope equipped with a Mettler FP5 hot stage.

X-ray diffraction was performed as follows. The CuK_α radiation from a 18 kW rotating anode X-ray generator (Rigaku-200) was selected by a flat germanium (1 1 1) monochromator delivering a $1\,mm^2$ beam onto the sample. The scattered radiation was collected on a two-dimensional detector (Imaging Plate system purchased from Mar Research, Hamburg). The sample-to-detector distance was 830 mm through helium, in order to reduce absorption and diffusion. The instrumental resolution was about 7×10^{-3} Å^{-1} (FWHM). Lindemann tubes ($\Phi = 1$ mm) were filled by capillarity from the isotropic phase without any alignment procedure. They were placed in an oven, the temperature of which was controlled within 10 mK. The tube axis could be either vertical or perpendicular to the beam. Exposure times were 30 min.

Helical pitch measurements were made in the following way. The SmC* phase can be studied by the well known and previously described Grandjean–Cano method using prismatic cells where the liquid crystal orients in a pseudo-homeotropic fashion [3, 13]. This method is not convenient for the SmC_A^* phase because it does not adopt a good orientation and the pitch shows large variations with temperature. Therefore the pitch measurements were performed by spectral analysis of the selective reflection on light ($\lambda = np$), using a 270 M, Jobin-Yvon-spectrometer (spectral range 0·4–1·7 μm). A very good accuracy was obtained for pitch values between 0·27 and 1·1 μm. The characterization of the SmC_α^* phase was performed on a very thin pseudo-homeotropic drop, where Friedel fringes could be seen. These fringes result from ellipticity variations of the propagating light [13, 14].

Electric field dependent properties were investigated using commercially available cells (E.H.C., Japan). These cells had been coated with indium tin oxide over a $0{\cdot}16\,cm^2$ active area. Their inner surfaces were also covered with a uni-directionally rubbed polyimide layer. The thickness of the cells was 6 μm. A classical electro-optical set-up was used for the measurement of switching current and apparent tilt angle [15].

3. Results

3.1. *Series IB or nCTBB8**

3.1.1. *Phase assignment*

The mesomorphic properties (transition temperatures and enthalpies) are summarized in table 1. Phase assignment was established by textural identification as described in previous papers related to AFLC compounds (see for example [3]). Most of the members of this series exhibited antiferroelectric phases. As observed many times [3–5], the shortest chain members displayed only a SmA phase. The classical regular decrease of the clearing temperatures with chain length increase was also observed.

The octylcarbonyloxy (8CTBB8*) (or nonanoyloxy) derivative merited particular interest because of the uncertainty concerning the nature of the high temperature smectic C phase. A simple textural observation did not permit us to distinguish a SmC* from a SmC_α^* phase. To perform miscibility studies, a binary phase diagram using this compound and the $n = 9$ derivative, presenting a larger variety of phases, was established (figure 1). The SmC* phase does exist for all compositions rich in the $n = 9$ compound but seems to

Table 1. Transition temperatures (°C) and, in italics, enthalpies (kJ mol^{-1}) for compounds of series IB.

n	Cr		SmI_A^*		SmC_A^*		SmC_{FI1}^*		SmC_{FI2}^*		SmC*		SmC_α^*		SmA		I
6	•	79·6	•	(77)	—		—		—		—		—		•	138	•
		28		*3·6*												*4·2*	
7	•	101·6	•	(82)	—		—		—		—		—		•	139	•
		35·8		*4*												*4·3*	
8	•	76	•	79	•	88	•	89	•	92·8	—		•	96·8	•	133	•
		27		*3·7*		*0·010*		*0·006*		*0·004*				*0·09*		*4·1*	
9	•	63·8	•	72·7	•	88	•	89	•	93·6	•	101	•	103·3	•	131·4	•
		14		*2·7*		*0·008*		*0·0005*		*0·017*				*0·12***		*3·6*	
10	•	68	•	(60·4)	•	84	•	85	•	90·5	•	106·8	•	107	•	128·5	•
		19		*2·4*				*0·015**		*0·026*				*0·19***		*3·0*	
11	•	81	•	(65·5)	•	89·6	—		•	93	•	111	—	—	•	127	•
		41		*3·0*		*0·026*		—		*0·026*		*0·26*				*4·8*	

* The sum of SmC_A^*–SmC_{FI1}^* and SmC_{FI1}^*–SmC_{F12}^* transition enthalpies.
** The sum of SmC^*–SmC_α^* and SmC_α^*–SmA transition enthalpies.

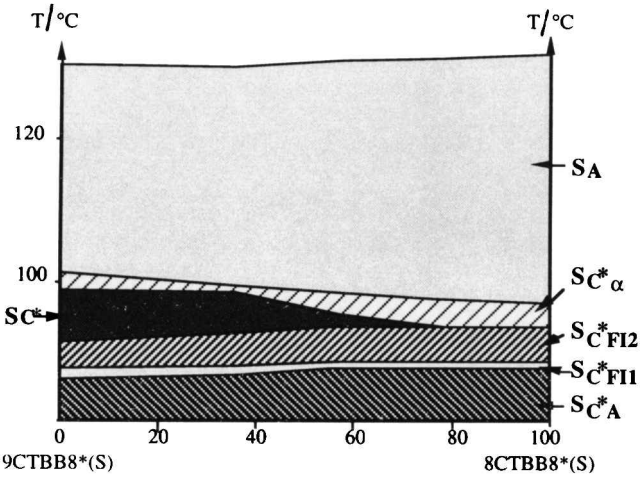

Figure 1. Isobaric binary diagram (in wt %) between the $n=8$ (right) and $n=9$ (left) numbers of series IB.

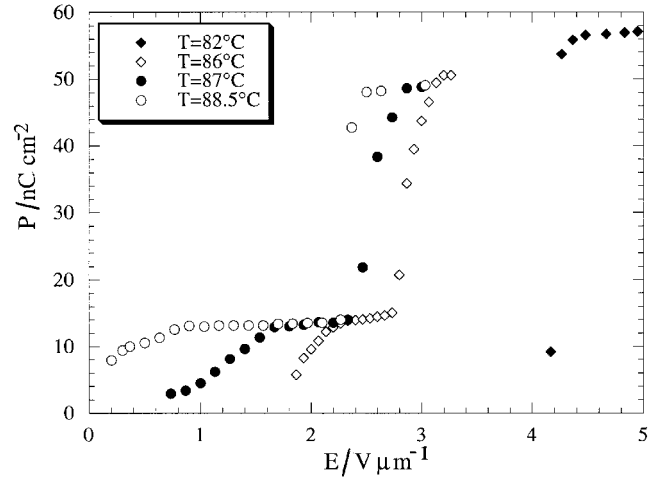

Figure 2. Polarization versus applied field for IB ($n=8$) (cell thickness: 6 µm, $\nu=50$ Hz).

disappear above 80 wt % of the $n=8$ compound. The lack of any SmC* phase was checked by performing helical pitch measurements on this latter compound. Friedel fringes typical of a SmC^*_α phase could be seen on a thin homeotropic drop at 95·3°C; the calculated pitch was 0·04 µm. On cooling the sample, these fringes develop into highly contrasted wire-like defects, as previously observed for a SmC^*_{FI} phase [5]. At lower temperatures, the SmC* phase appears to be very dark with red coloured defects. The value of the pitch could be calculated through the formation of Grandjean–Cano defects in a prismatic cell. The pitch was 0·45 µm at 89°C.

3.1.2. *Electro-optic studies*

Electro-optical studies were also performed on the $n=8$ derivative sample. Because of the lack of any SmC* phase, the material seemed to be a good candidate to investigate further the behaviour of the SmC^*_{FI} phase under an applied electric field. Moreover, its unusually wide range SmC^*_α could permit a study of this phase at several temperatures. The polarization versus the applied electric field was recorded at several temperatures in the different smectic C phases (figure 2). As usual, it was necessary to apply a threshold field to induce a polarization in both SmC^*_A and SmC^*_α phases. The threshold field decreased with the temperature in the SmC^*_A phase whereas it remained constant in the SmC^*_α phase. In this latter case, the minimal field required to induce a measurable polarization could not be called 'threshold' because no saturated ferroelectric state could be reached in the SmC^*_α phase [16]. In the two SmC^*_{FI} phases, the threshold field was no longer detected and the polarization versus the applied field showed a plateau as already observed in SmC^*_{FI} phases for other compounds [3, 4]. It was suggested that the SmC^*_{FI} phases could correspond to the coexistence of the surrounding phases, i.e. the SmC^*_A and SmC* phases [17]. Despite the absence of any SmC* phase, the intermediate plateau was observed. Its values remained constant at about 1/4 of the maximum polarization. This value was also shown to be independent of the thickness of the cell (figure 3). This seems to rule out any strong influence of the anchoring to the cell surfaces. It has sometimes been argued that SmC^*_{FI} phases could be mixtures of microdomains of both SmC* and SmC^*_A phases. If this statement is true, such microdomains could not be induced by the cell surfaces.

3.2. *Series IC or nCT BB9**

3.2.1. *Phase assignment*

Transition temperatures and enthalpies for the compounds IC are summarized in table 2. This table also includes the mesomorphic sequences obtained for two of the racemic analogues. The mesomorphic behaviour of this series is very different from that of the previous series and from that of most other conventional AFLC materials.

Most of the compounds presented the same textures when viewed by polarizing microscopy. On cooling down from the isotropic liquid, the classical texture of a SmA phase was observed for the shortest chain members ($n=8$–12). A smooth extinct texture could be obtained by using a planar alignment procedure. On further cooling, many additional elliptic-shape defects appeared suddenly. In homeotropic samples, uniform domains remained fairly dark for $n=8$–10. For $n=11$ and 12, they became suddenly green and blue, respectively. This indicates the presence of a helix, which is the signature of a C-type smectic phase. The longest derivatives ($n=14$ and 16) did not exhibit any SmA phase and a direct transition from the isotropic liquid to a brightly coloured texture was seen. On cooling at a very slow

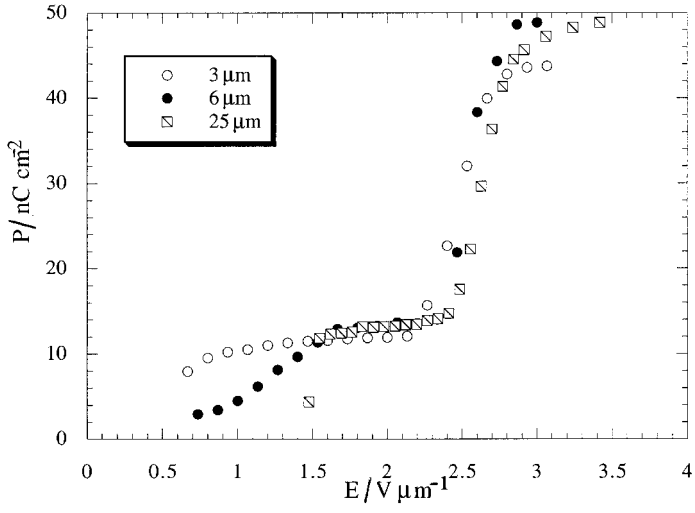

Figure 3. Polarization versus applied field for IB ($n = 8$) at 87°C with different cell thicknesses.

Table 2. Transition temperatures (°C) and, in italics, enthalpies (kJ mol^{-1}) for compounds of series IC.

n	Cr		SmI_A^*		SmC_A^*		SmA		L		I
8	•	<50	•	68·5	•	82·6	•	106·9	—		•
				2·25		*0·24*		*3·36*			
9	•	<50	•	61·2	•	81·9	•	105·2	—		•
				1·89		*0·39*		*2·37*			
10	•	56·4	•	56·9	•	81·7	•	96·9	•	?	•
		34·8		*2·47*		*0·43*		*1·72*			
11	•	74·3	•	(58·4)	•	81·1	•	93·4	•	≈96	•
		44·1		*3·74*		*0·54*		*1·35*			
12	•	80·1	•	(62·2)	•	83·0	•	91·7	•	≈97	•
		49·6		4·92		0·68		*0·94*			
14	•	81·6	•	(65·3)	•	(80·8)	—		•	≈97	•
		52·3		*8·2*		*1·14*				*2·6*	
16	•	81·3	•	(68·5)	•	(79·8)	—		•	≈96	•
		54·6		*12·0*		*1·14*				*3·5*	
8 (RAC)	•	<50	•	69·3	•	82·0	•	108·0	—		•
				2·5		*0·22*		*3·65*			
16 (RAC)	•	75·8	•	(69·3)	•	84·7	•	93·0	—		•
		44·4		*12·1*		*0·84*		*3·46*			

rate for these two latter compounds, i.e. less than 0·1°C min^{-1}, one could see concentric coloured rings rapidly growing around nucleating spots. To determine the exact nature of this smectic C phase, the isomorphy with a reference sample was checked using the contact method with the octyloxy derivative of series IA. The SmC phase was found to be continuously miscible with the SmC_A^* phase of the reference compound over the whole concentration range. The tilted bilayer character of this smectic phase could be confirmed by investigation of the phase displayed by some analogous racemic compounds. Two derivatives were synthesized and their liquid crystalline behaviour analysed using optical microscopy. Both showed a texture with two-branch 'schlieren' defects ($s = 1/2$), which is typical of a SmC_A phase [18].

It is surprising to note that the SmA–SmC_A^* transition was a first-order transition. Whereas it is usually difficult to locate SmC*–SmC_α^* or SmC*–SmA transitions for AFLC compounds because of small texture changes and small transition enthalpy values, a large enthalpy (table 2) and a drastic textural change are associated with the direct transition from SmC_A^* to SmA. This first-order character is even more pronounced as the flexible chain length increases.

On further cooling, for all members of this series, a more ordered phase was detected at low temperatures. It could be identified as a SmI_A^* because of its mosaic-like texture with many grey defects in pseudo-homeotropic domains and transverse striations in the focal-conic defects.

3.2.2. *Thermal behaviour*

For the above reported phases, perfect agreement was found between the transition temperatures detected by

DSC and optical microscopy. In addition, DSC analysis revealed the occurrence of a thermal event at a temperature higher than the clarification point for most of the compounds (figure 4). Isotropization seemed to take place in two ways. For the short chain derivatives (above $n = 10$), only a bump could be seen on the right side of the clearing peak instead of a return to the baseline, but a well-defined broad peak could be detected for the longest chain derivatives. This seems to indicate the existence of a fourth mesophase just below the isotropic liquid state. Attempts to detect it by optical microscopy failed, even by using classical alignment procedures. A similar phenomenon occurring in the isotropic temperature range was previously reported for some chiral liquid crystalline systems involving a TGB_A phase [11, 12]. We will continue with the nomenclature introduced by these authors and our fourth phase will be called L.

As shown in figure 4, the shape of the transition peak from L to the liquid state was rather broad and

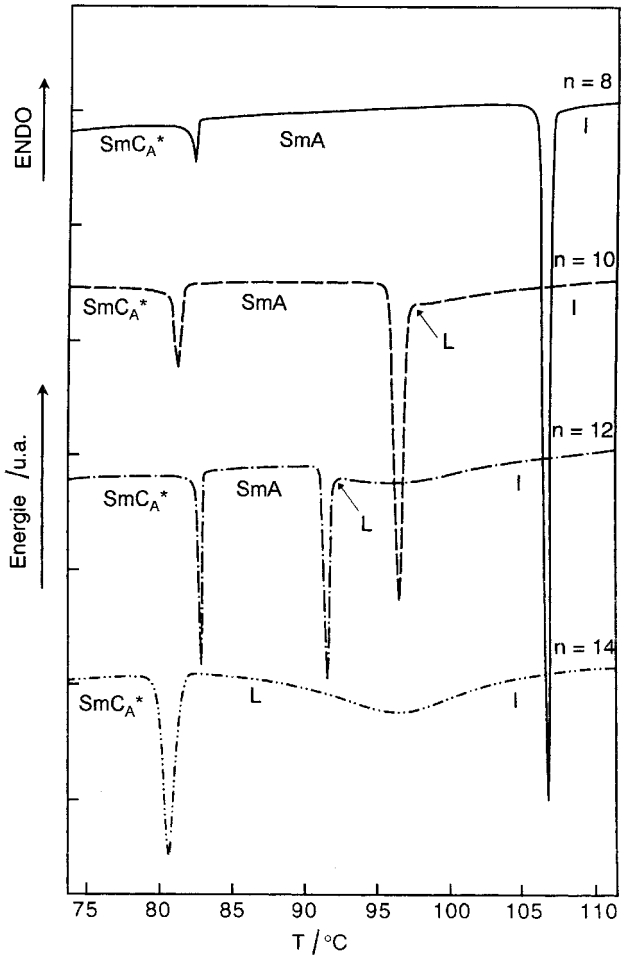

Figure 4. DSC diagrams for cooling scans (3°C min^{-1}) of the IC compounds with different chain lengths.

the transition did not occur at a precise temperature. Furthermore the maximum of the peak seemed to be located at a constant temperature independent of the chain length. For $n = 10$–16, the L–I transition only oscillated between 95 and 97°C. Meanwhile, the SmA–L temperatures decreased with increase in the number of flexible units. Therefore, the longer the chain length, the more stable the L phase. This is not surprising, as decrease in clearing temperatures as molecular length increases is a classical behaviour for rod-like compounds. For the same reason, the SmA range progressively decreased until it disappeared completely and a direct SmC_A^*–L transition occurred. The SmC_A^*–SmA temperatures remained approximately constant.

Comparison of the mesomorphic behaviour of enantiomeric and racemic samples clearly indicated the relation between the existence of the L phase and the optical activity of the compounds (table 2). For the $n = 8$ compound which did not exhibit any L phase, the transition temperatures obtained for both racemic and chiral derivatives were similar. On the contrary, the sequences obtained for the $n = 16$ derivatives were rather different. The wide L phase displayed by the $n = 16$ chiral derivative was no longer observed for its racemic analogue. Instead, a SmA phase was present but the SmC_A–SmA transition occurred at a much higher temperature than the SmC_A^*–L transition (84·7°C instead of 75·1°C). This shift could be partly explained by the higher crystallinity of the enantiomeric compound, as indicated by the very different melting temperatures.

3.2.3. *Optical investigations*

3.2.3.1. *Pitch measurements in the SmC_A^* phase*. The helical pitch of the SmC_A^* phase was studied for all compounds of series IC. Similar results were obtained on cooling or heating; only results obtained on cooling will be presented here. The selective reflection was analysed with pseudo-homeotropic flat drops deposited on glass slides.

For $n = 8$ in series IC, the SmA–SmC_A^* transition occurs at 83·5°C; the pitch was then 0·67 μm. Upon further cooling it rapidly increases to 1·1 μm at 78°C (upper limit of our spectrometer range); the extrapolated value at the SmC_A^*–SmI_A^* transition (71·2°C) was larger than 2 μm.

A similar behaviour was observed for the other compounds (figure 5). The main values, summarized in table 3, show large pitch variations with an amplitude decreasing with the chain length: for $n = 14$ the pitch does not vary very much; it is quasi-constant for $n = 16$. The chain length also played an important role in the pitch values which are shorter for larger n.

3.2.3.2. *Optical observations on the liquid-like L phase.* Very strange phenomena could be observed on very thin drops when the sample was in its liquid state above the

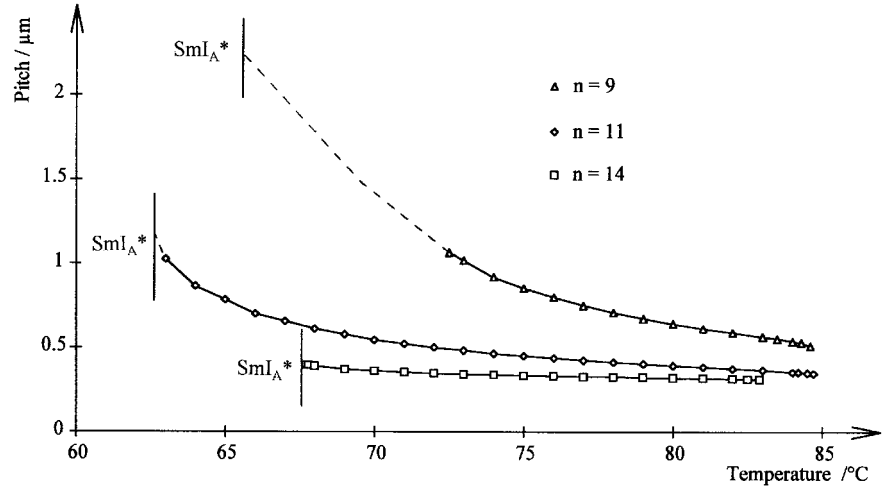

Figure 5. Temperature dependence (°C) of the helical pitch (µm) in the SmC_A^* phase. Measurements were performed on cooling by spectral analysis of the selective reflection of light.

Table 3. Pitch values in the SmC_A^* phase near the low and high transition temperatures for series IC.

	SmC_A^*–SmI_A^*		SmC_A^*–SmA or $L_{(1)}$	
n	*T*/°C	*P*/µm	*T*/°C	*P*/µm
8	71·2	>2	83·5	0·67
9	65·5	≈2	84·6	0·51
10	61	≈1·6	83·7	0·36
11	62·5	1·2	84·7	0·35
12	63·9	0·65	84·5	0·31
14	67·7	0·4	82·9	0·31
16	70·5	0·31	78·7	0·31

SmC_A^* and SmA phases. The derivatives with $n = 8$ and 9 do not present the L phase and no peculiar texture occurs for these compounds in the I phase. The situation is different for the other members of the series.

For $n = 10$–12, the SmC_A^* homeotropic phase shows typical selective reflection colours and numerous Grangjean–Cano threads. At the $SmC_A^* \rightarrow$ SmA transition, the sample remained homeotropic. It was dark grey when observed between crossed polarizers, and presented linear thin defects which are often generated by Grandjean–Cano threads. These defects progressively turned into wider 'schlieren' where an intense Brownian motion could be observed. The SmA → L transition is visible through the appearance of drops of increasing size. The schlieren defects remained visible in the liquid-like L phase and their contrast progressively diminished when the sample was heated up to the I phase.

For $n = 14$ and 16, the SmC_A^* phase directly transformed into L. The Grandjean–Cano threads of the SmC_A^* phase, and schlieren of the L phase frequently developed at the same place, very often in a circulating manner. This phenomenon seems to show that the presence of schlieren in the L phase could be related to the winding up (figure 6) of the SmC_A^* phase.

For $n = 16$, three events could be seen in the L phase. They seemed to occur at well defined temperatures. When approaching these temperatures, the Brownian motion became more intense and the smooth schlieren suddenly transformed into streaked schlieren, that immediately transformed again into smooth schlieren (figure 7). Such an event occurred three times in the L phase of the $n = 16$ compound; it was not detected for other compounds. The transition temperatures are given below:

Heating: SmC_A^* 80·3 $L_{(1)}$ 81 $L_{(2)}$ 82·2 $L_{(3)}$ 85·7 $L_{(4)}$ 97 I

Cooling: SmC_A^* 79·8 $L_{(1)}$ 80·2 $L_{(2)}$ 81·4 $L_{(3)}$ 85·2 $L_{(4)}$ 96 I

Unlike the $L_{(x)} \leftrightarrow L_{(y)}$ transformations that occurred at precise temperatures, the L↔I transformation was progressive; the given L–I temperatures are those corresponding to a change in the schlieren contrast. It is difficult at present to give any interpretation of these optical events occurring in the L phase (or several phases?). Such schlieren textures have also been observed in the anomalous isotropic L phases of other chiral systems, namely with TGB_A–L–I [11], N*–BP–I [19], TGB–BP–I [20]; the L phase of our present derivatives (with the SmC_A^*–L–I sequence) probably presents strong analogies with the BPIII phase.

3.2.4. *Electro-optic studies*

The electric response of the SmC_A^* phase to an applied electric field was recorded. A triangular shaped signal was applied to the surface of the cells. As shown in figure 8, four current peaks were detected over a full period, indicating four transitions. At zero current, the liquid crystal was in its antiferroelectric state (AF) and tilting directions were opposite from one layer to the next. As the applied field reached a sufficient value, a transition to a ferroelectric state occurred (FO^+) and a current peak could be detected. The reverse transition

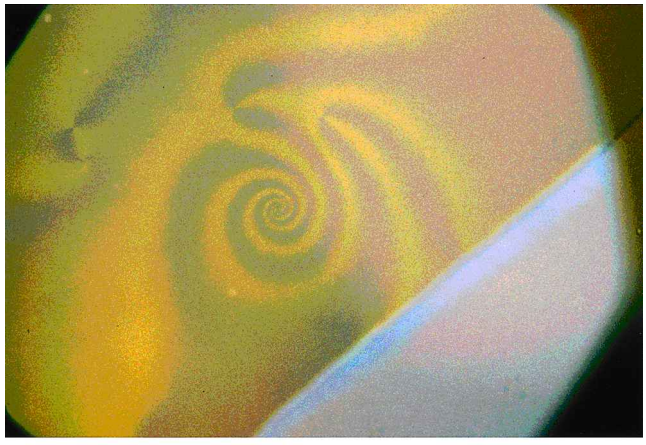

(*a*)

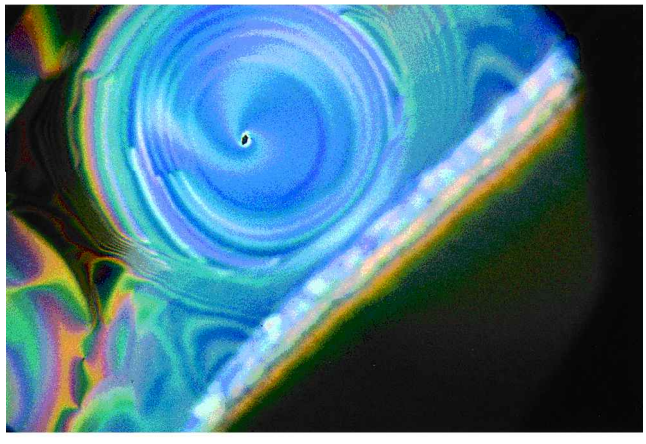

(*b*)

Figure 6. Optical microscopic textures of very flat pseudo-homeotropic drops of IC ($n=16$). (*a*) $L_{(1)}$ phase; (*b*) $L_{(1)}$–SmC_A^* transition.

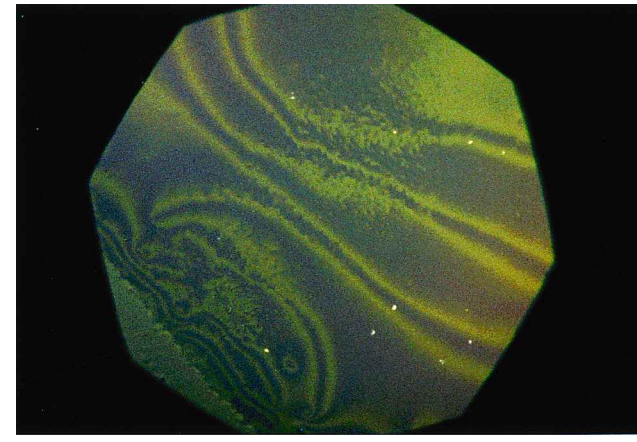

(*a*)

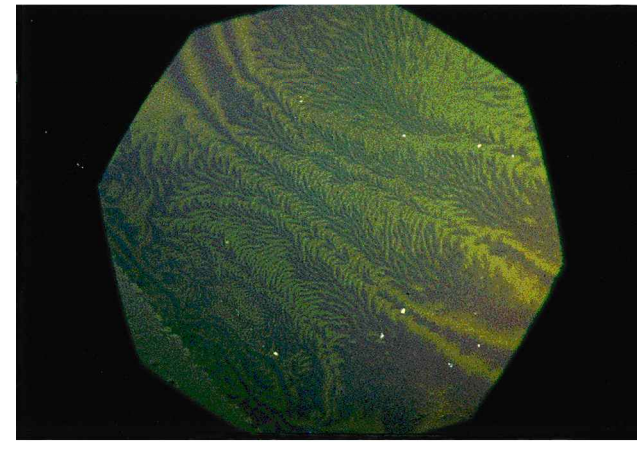

(*b*)

Figure 7. Transformation between the $L_{(3)}$ and $L_{(4)}$ states of IC ($n=16$) visualized on a flat homeotropic drop. (*a*) Smooth schlieren observed in the $L_{(3)}$ phase; in the centre of the picture, we distinguish the beginning of the transformation. (*b*) Between the $L_{(3)}$ and $L_{(4)}$ states ($T=85{\cdot}7°C$). The smooth schlieren of the $L_{(3)}$ phase suddenly transform into streaked schlieren; after this, the streaked schlieren immediately transform again into smooth schlieren, the $L_{(3)}$ and $L_{(4)}$ textures are absolutely alike.

could be observed on decreasing the applied field. When applying negative values of the voltage, the same phenomenon occurred, but the tilt angle in the ferroelectric state was opposite to that previously observed (FO^-). This behaviour is typical of that from a SmC_A^* phase, therefore confirming its nature.

Threshold fields were measured for the $n=8$ and $n=12$ compounds in series IC. For both compounds, the threshold field decreased with increasing the temperature, and was higher for the $n=12$ derivative than for $n=8$, indicating a better stability of the SmC_A^* phase for a longer chain compound.

Ferroelectric properties under saturation conditions were also measured for these compounds (figure 9). As was already noted elsewhere [4], polarization was higher for the longer derivative. It should also be noted that the $n=12$ compound undergoes a strong electroclinic effect far in the SmA phase. Polarization remains non-negligible even 3°C above the SmC_A^*–SmA transition.

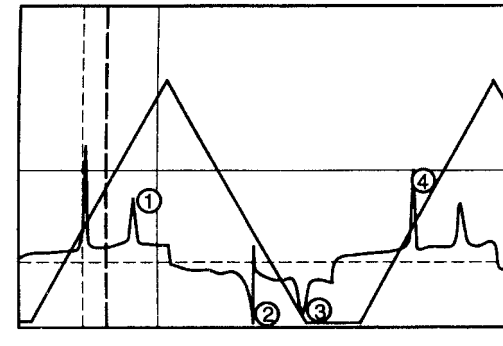

Figure 8. Polarization current versus field with triangular form for IC ($n=12$) at 80°C.

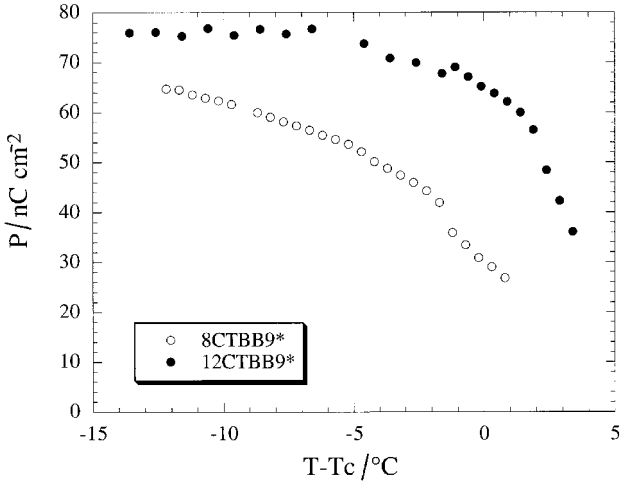

Figure 9. Polarization (nC cm^{-2}) versus temperature (°C): ($\nu = 50$ Hz). $E = 9$ V μm^{-1} for IC ($n = 8$); $E = 20$ V μm^{-1} for IC ($n = 12$).

4. Discussion

4.1. *Effect of the linkage between the non-chiral chain and the rigid core on the liquid crystalline behaviour*

The synthesis and characterization of series IB and IC was aimed at investigating the role of two major structural modifications. The first one concerns the nature of the linkage between the flexible chain and the rigid core. This was investigated by comparing the liquid crystalline behaviour of series IB with that of series IA, which was reported in detail elsewhere [4]. Like MHPOBC [1], the tolane-based series IA has its flexible chain attached to the rigid part through an ether linkage. Although some compounds bearing a different linkage were previously known [21, 22], no systematic study had been reported and the role of this particular linkage remained unknown. A comparison between series IA and IB might help to clarify the importance of such a parameter. Replacement of the ether linkage by an ester group did not however modify the general liquid crystalline behaviour. These antiferroelectric compounds exhibit a wide variety of liquid crystalline phases, most of them displaying a rich polymorphism including the sequence SmC^*_A–SmC^*_{FI1}–SmC^*_{FI2}–SmC*–SmC^*_α–SmA. The trend in stability of these phases with the flexible chain length also appeared to be similar to that of series previously reported. The shortest chain members did not show any tilted smectic phase. The SmA and SmC^*_α phases followed a similar evolution. Their stability decreased by increasing the molecular length. The SmC^*_α phase disappeared when $n = 11$.

We have shown in a previous paper [5] that the SmA and SmC^*_α phases are very sensitive to the longitudinal polarity of the antiferroelectric compound. An increase of the longitudinal dipole moment of the rigid core in the area close to the non-chiral chain could stabilize the SmA and SmC^*_α phases. When both of them were too strongly stabilized, the SmC^*_A phase was found to disappear.

Comparison of the stability of SmA and SmC^*_α phases for series IA and IB could be relevant to the role of the linkage between the flexible chain and the rigid core, since the replacement of an ether linkage by an ester group also modifies the longitudinal polarity of the molecule. Table 4 reports the SmA ranges for these two series. The SmA range of series IB is always larger than for series IA. This comparison is better made between chain lengths with $(n+1)$ units for series IA and with n units for series IB, because of the presence of an additional carbon due to the COO group in the latter case. In this situation, the stabilization of the SmA phase for series IB is even more pronounced. Therefore, it seems that a longitudinal polarity change is at the origin of the different liquid crystalline behaviours of series IA and IB. The nature of the linkage between the flexible chain and the rigid core appears to be important because it can modify the longitudinal polarity in this area of the chemical structure.

4.2. *Importance of the chiral moiety on the stability of the SmC^*_A phase*

It seems that the chemical modification performed on the chiral chain had more influence on the liquid crystalline behaviour of these compounds. The replacement of the methyl group attached to the chiral carbon by an ethyl group appears strongly to stabilize the SmC^*_A phase. The rich polymorphism generally obtained for AFLC compounds is no longer observed. All helical smectic phases usually present between the SmC^*_A and SmA phases, i.e. the SmC^*_{FI}, SmC* and SmC^*_α, disappear and the SmC^*_A–SmA transition is instead first-order. Similar trends have been reported for AFLC compounds bearing different chiral chains. A direct SmC^*_A–SmA transition was observed when the side group on the asymmetric carbon was a CF_3 or C_2F_5 group [8]. It seems that the size of the short chiral group is an important parameter. Nishiyama *et al.* [9] studied the

Table 4. Domain existence of SmA for IA and IB derivatives.

	ΔT (SmA)	
n	Series IA	Series IB
7	37·6	57
8	29·8	37·2
9	21·1	28·1
10	17·4	21·5
11	10·6	16
12	8·1	

effect of the shorter chain length on a series of benzoate–biphenyl based AFLC compounds. They also obtained a direct SmC_A^*–SmA transition with a propyl group, but not with ethyl. The side chiral group has to be big enough to induce this direct transition. The size of the short chain which is necessary to achieve a direct transition from SmC_A^* to SmA might be related to the ability of the rigid core structure itself to favour antiferroelectric phases. It should be noted here that the series investigated by these authors involved a biphenyl ring system close to the chiral moiety, which is less favourable to antiferroelectric phases than our tolane–benzoate series [5]. Therefore, the size of the short group linked to the asymmetrical carbon seems to be a fundamental parameter for the kind of AFLC structure investigated here.

This importance was confirmed by measuring the interlayer spacing for smectic phases of series IB and IC. X-ray diffraction experiments were performed over the whole temperature range of smectic phases for the $n = 8$ derivatives from both series. These two compounds have a similar chemical structure, except for the size of the short chiral chain. Figure 10 shows the plot of the smectic spacings versus temperature for these two compounds. The layers had an approximately constant thickness over the SmA range, except at temperatures close to the clearing point because of strong thermal fluctuations. The transition from the SmA phase to a tilted smectic phase was clearly indicated by the abrupt decrease in the layer spacing. Both compounds exhibited similar phase evolutions, but the smectic period was always smaller for the IB derivative (the SmA layers are 1 Å thinner than for the IC compound). As the layer thickness was close to the molecular length, this seems to indicate that the additional methyl group associated with the asymmetrical carbon contributes to the mesogen length. The shorter chain linked to the chiral carbon might not lie in a direction perpendicular to the long axis of the molecule. This would be consistent with results obtained from the crystalline state [23, 24], which showed that the long tail of the chiral chain was rather perpendicular to the long axis of the molecule. Therefore, the short moiety of the chiral chain could interact with the tails of the molecules in an adjacent smectic layer. It seems that an increase in the size of this group could increase some specific antiferroelectric interactions and induce a direct transition from a SmA to SmC_A^* phase. This would also mean that other helical smectic phases usually observed for AFLC compounds would result from a competition between ferro- and antiferro-electric-type molecular interactions.

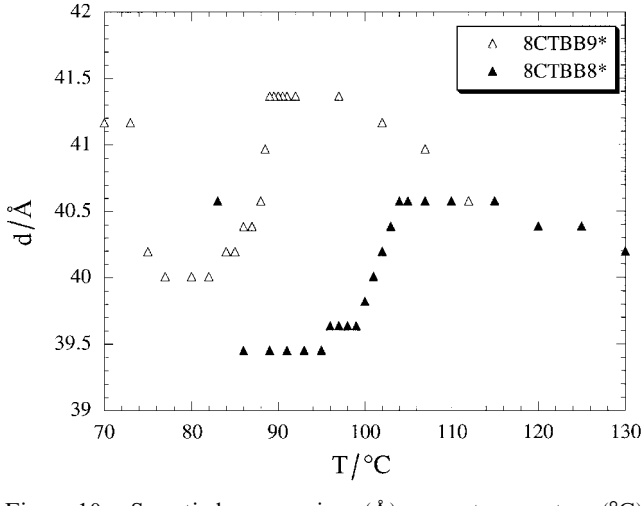

Figure 10. Smectic layer spacings (Å) versus temperature (°C) for compounds IB ($n = 8$) and IC ($n = 8$).

4.3. *Isotropic phenomena*

The second interesting point observed with this series concerns the special clearing behaviour. It was shown that a 'liquid-like' phase could appear above the clearing temperature. This phase could be observed only for chiral compounds, and racemic analogues displayed just a SmA phase in the same range of temperature. Because of this observation and the presence of helical defects, we conclude that the new phase is linked to the chirality of our compounds. However, the thermal behaviour reminds us of other particular transitions, which have not been fully understood so far. The particular shape of the transition peaks for the sequence SmA–L–I was rather similar to the sequence Blue Phase I–Blue Phase III–I [19] or above a cubic D phase [25–27]. For these latter systems as well in systems involving a TGB_A phase [11, 12], the existence of an intermediate phase prior to isotropization has been supposed to be due to the presence of isolated entities after the melting of a network [28]. For the Blue Phase I, the twisting defects are organized on a three-dimensional network. The BPIII, the so-called Blue Fog phase, could be constituted of twisting cylinders. In cubic-D systems, the small species are molecular aggregates packed in a cubic fashion. The intermediate phase would be micellar in this case, but it is totally different to the smectic Q phase in the sequence SmC_A^*–Q–I [29]. For the TGB phases, after the melting of the grain boundary defects, the liquid-like L phase could be constituted from isolated smectic blocks and their transition to an isotropic state could occur later. The first sharp transition peak could correspond to the melting of the network and molecules could remain as isolated associates; the second broad peak would then correspond to a progressive disappearance of the short range effects, leading to the isotropic liquid.

Such a transition to the isotropic phase has been confirmed for blue phase systems but not for the others: recent experimental [30–32] and theoretical [33] work

has shown that the BPIII–I transition can be first order and end in a critical point, and that above this point, the fluids show a supercritical conversion from BPIII to I accompanied by a broad DSC peak. This behaviour confirms that BPIII and I phases have the same symmetry. Such proof has not yet been obtained for the other systems, for which the above description seems nevertheless a reasonable hypothesis.

Our studies have shown for the first time the existence of this kind of liquid-like phase for antiferroelectric compounds. The liquid-like L phase was found to be more stable as the chain length increased. At the same time, it was seen that the SmC_A^* phase too was stabilized; the first-order character of the SmC_A^*–SmA transition increased and the threshold field necessary to destroy the antiferroelectric structure was higher as the chain length increased. Antiferroelectric interactions seemed to be reinforced as the flexible chain length in these compounds increased. The simultaneous stabilization of the SmC_A^* and L phases could indicate that the strength of the antiferroelectric interactions was of some importance to the appearance of the L phase. One could therefore imagine that this L phase corresponds to isolated aggregates allowing an antiferroelectric pairing of the molecules. The SmA–L transition would then correspond to the disappearance of the periodic layering. However, the existence of liquid-like defects above the SmC_A^* phase in series IC seems to be related to its particular chirality. Indeed, it appeared when the chiral moiety was chemically modified. This would be consistent with the analogy to the BPIII phase, the existence of which could be favoured in a certain range of chirality.

5. Materials

The following sections give details of individual steps in the synthesis of the IC compound 10CTBB9*.

5.1. *(S)-2-Ethylheptyl 4-benzyloxybenzoate (**2**)*

To a solution of (*S*)-3-nonanol (4·5 g, 34 mmol) in CH_2Cl_2 (50 ml) was added DCC (7·8 g, 37 mmol), DMAP (0·4 g) and 4-benzyloxybenzoic acid (8·44 g, 37 mmol). This mixture was stirred at room temperature overnight, filtered, the solvent evaporated and the residue purified by chromatography on silica gel using a mixture of heptane and ethyl acetate (9 : 1) as eluent. Yield: 12 g, 80%. ^{1}H NMR ($CDCl_3$): δ (ppm) = 0·85 (t, 3H, CH_3), 0·95 (t, 3H, CH_3), 1·3 (m, 8H, $4CH_2$), 1·6–1·8 (m, 4H, $2CH_2$), 5 (s, 2H, CH_2–O), 5·1 (m, 1H, O–CH), 6·9 (d, 2H arom.), 7·3 (m, 5H arom.), 7·95 (d, 2H arom.). IR: 2927, 2856, 1683, 1607, 1280, 1166, 1112, 851, 773 cm^{-1}.

5.2. *(S)-2-Ethylheptyl 4-hydroxybenzoate (**3**)*

To a solution of the oil **2** (12 g, 28 mmol) obtained above in a mixture of ethyl acetate and ethanol 95% (4 : 1) was added 0·6 g of 10% Pd/C. Hydrogen was added under a slight pressure; hydrogen consumption stopped after two hours. The catalyst was then filtered off and the solvent evaporated. The liquid phenol was rapidly purified on silica gel using a mixture of heptane and ethyl acetate (75 : 25) as eluent. Yield: 6·25 g, 80%. ^{1}H NMR ($CDCl_3$): δ (ppm) = 0·85 (t, 3H, CH_3), 0·95 (t, 3H, CH_3), 1·3 (m, 8H, $4CH_2$), 1·6–1·8 (m, 4H, $2CH_2$), 5·1 (m, 1H, O–CH), 6·9 (d, 2H arom.), 7·95 (d, 2H arom.). IR: 3357, 2927, 2856, 1683, 1607, 1280, 1166, 1112, 851, 773 cm^{-1}.

5.3. *(S)-2-Ethylheptyl 4-(4-iodobenzoyloxy)benzoate (**4**)*

This compound was obtained following the synthetic route described for compound **2** using the phenol **3** (6·2 g, 23 mmol), DCC (5·32 g, 26 mmol), DMAP (0·26 g) and 4-iodobenzoic acid (6·4 g, 26 mmol) in 50 ml of CH_2Cl_2. The ester obtained was purified by chromatography on silica gel using a mixture of heptane and ethyl acetate (9 : 1) as eluent. Yield: 10·1 g, 87%. ^{1}H NMR ($CDCl_3$): δ (ppm) = 0·85 (t, 3H, CH_3), 0·95 (t, 3H, CH_3), 1·3 (m, 8H, $4CH_2$), 1·6–1·8 (m, 4H, $2CH_2$), 5·1 (m, 1H, O–CH), 7·3 (d, 2H arom.), 7·9 (2d, 4H arom.), 8·1 (d, 2H arom.). IR: 2917, 2857, 1751, 1716, 1588, 1504, 1290, 890, 759 cm^{-1}.

5.4. *(S)-4-(2-Ethylheptyloxycarbonyl)phenyl 4-tetrahydropyranyloxytolane-4′-carboxylate (**5**)*

Into a 250 ml round-bottomed flask were introduced compound **4** (10 g, 20 mmol), 4-(1-tetrahydropyranyloxy)-phenylacetylene (4 g, 20 mmol) and triphenylphosphine (144 mg) in 40 ml of di-isopropylamine under a nitrogen flow. This mixture was stirred and heated to 30°C until complete dissolution occurred. Then 20 mg of $PdCl_2$ and 20 mg of $Cu(AcO)_2.H_2O$ were added as catalysts. The solution was heated up to 90°C and maintained at this temperature during 2 h. After cooling to room temperature, the salt was filtered off and washed with ethyl acetate. The solvent was evaporated and the solid was dissolved again in ethyl acetate and hydrolysed with 100 ml of acidified iced water. The organic phase was removed, washed with pure water and dried over anhydrous NA_2SO_4. This salt was then filtered off and the solvent evaporated. The product obtained was chromatographed on silica gel using a mixture of heptane and ethyl acetate (9 : 1) as eluent. It was finally recrystallized from ethanol. Yield: 7·92 g, 70%, m.p. 53°C. ^{1}H NMR ($CHCl_3$): δ (ppm) = 0·85 (t, 3H, CH_3), 0·95 (t, 3H, CH_3), 1·3 (m, 8H, $4CH_2$), 1·6–1·8 (m, 6H, $3CH_2$), 1·8–2·1 (m, 4H, $2CH_2$), 3·65 (m, 1H, THPO), 3·9 (m, 1H, THPO), 5·1 (m, 1H, O–CH), 5·5 (s, 1H, THPO), 7·05 (d, 2H arom.), 7·3 (d, 2H arom.), 7·5 (d, 2H arom.), 7·65 (d, 2H arom.), 8·15 (2d, 4H arom.). IR: 2917, 2857, 1751, 1716, 1588, 1504, 1290, 890, 759 cm^{-1}.

5.5. *(S)-4-(2-Ethylheptyloxycarbonyl)phenyl 4-hydroxytolane-4′-carboxylate (**6**)*

Compound **5** (7·8 g) was dissolved in a mixture of CH_2Cl_2 (40 ml) and methanol (60 ml) and 4-toluensulphonic acid (PTSA) (160 mg) was added to the solution, which was stirred at room temperature during one hour. The solvent was then evaporated and the phenol was chromatographed on silica gel using a mixture of heptane and ethyl acetate (75:25) as eluent. Yield: 5·75 g, 85%. ^{1}H NMR ($CDCl_3$): δ (ppm) = 0·85 (t, 3H, CH_3), 0·95 (t, 3H, CH_3), 1·3 (m, 8H, $4CH_2$), 1·6–1·8 (m, 4H, $2CH_2$), 5·1–5·3 (m, 2H, O–CH and OH), 6·9 (d, 2H arom.), 7·3 (d, 2H arom.), 7·5 (d, 2H arom.), 7·7 (d, 2H arom.), 8·15 (2d, 4H arom.). IR: 3427, 2930, 2853, 1712, 1598, 1266, 1078, 765 cm^{-1}.

5.6. *(S)-4-(2-ethylheptyloxycarbonyl)phenyl 4-n-undecanoyloxytolane-4′-carboxylate (IC, n = 10)*

This compound was obtained following the synthetic route described for compound **3** and using phenol **6** (0·49 g, 1 mmol), DCC (0·23 g, 1·1 mmol), DMAP (0·01 g) and undecanoic acid (0·18 g, 1·1 mmol) in 20 ml of CH_2Cl_2. The product was purified by chromatography on silica gel using CH_2Cl_2 as eluent. It was recrystallized from absolute ethanol. Yield: 0·45 g, 70%. ^{1}H NMR ($CDCl_3$): δ (ppm) = 0·8–1·0 (m, 9H, $3CH_3$), 1·2–1·8 (m, 24H, $12CH_2$), 2·6 (t, 2H, CH_2), 5·2 (m, 1H, O–CH), 7·15 (d, 2H arom.), 7·3 (d, 2H arom.), 7·6 (2d, 4H arom.), 8·15 (2d, 4H arom.). $[\alpha]_D^{22} = +9·7°$ ($c = 1·66$, CH_2Cl_2).

We would like to thank Prof. G. Sigaud, Drs J. P. Marcerou and P. Barois and Prof. G. Joly for their interest in this work; also the Aquitaine and Nord-Pas de Calais regions and the FEDER for the funding of the high resolution X-ray diffractometer and the spectroscopic set-up used for smectic layer spacing and helical pitch measurements.

References

[1] Chandani, A. D. L., Ouchi, Y., Takezoe, H., and Fukuda, A., 1989, *Jpn. J. appl. Phys*, **28,** 1261.
[2] Goodby, J. W., and Chin, E., 1988, *Liq. Cryst*., **3,** 1245.
[3] Nguyen, H. T., Rouillon, J. C., Cluzeau, P., Sigaud, G., Destrade, C., and Isaert, N., 1994, *Liq. Cryst*., **17,** 571.
[4] Cluzeau, P., Nguyen, H. T., Destrade, C., Isaert, N., Barois, P., and Babeau, A., 1995, *Mol. Cryst. liq. Cryst*., **260,** 69.
[5] Faye, V., Rouillon, J. C., Destrade, C., and Nguyen, H. T., 1995, *Liq. Cryst*., **19,** 47.
[6] Nguyen, H. T., Twieg, R. J., Nabor, M. F., Isaert, N., and Destrade, C., 1991, *Ferroelectrics*, **121,** 187.
[7] Werth, M., Nguyen, H. T., Destrade, C., and Isaert, N., 1993, *Liq. Cryst*., **15,** 479.
[8] Suzuki, Y., Nonaka, O., Koide, Y., Okabe, N., Hagiwara, T., Kawamura, I., Yamamoto, N., Yamada, Y., and Kitzume, T., 1993, *Ferroelectrics*, **147,** 109.
[9] Nishiyama, I., and Goodby, J. W., 1993, *J. mater. Chem*., **3,** 149.
[10] Ouchi, Y., Yoshioka, Y., Ishii, H., Seki, K., Kitamura, M., Noyori, R., Takanishi, Y., and Nishiyama, I., 1995, *J. mater. Chem*., **5,** 2297.
[11] Nguyen, H. T., Babeau, A., Rouillon, J. C., Sigaud, G., Isaert, N., and Bougrioua, F., 1996, *Ferroelectrics*, **179,** 33.
[12] Goodby, J. W., Nishiyama, I., Slaney, A. J., Booth, C. J., and Toyne, K. J., 1993, *Liq. Cryst*., **14,** 37.
[13] Brunet, M., and Isaert, N., 1988, *Ferroelectrics*, **84,** 25.
[14] Laux, V., Isaert, N., Nguyen, H. T., Cluzeau, P., and Destrade, C., 1996, *Ferroelectrics*, **179,** 25.
[15] Dupont, L., Glogarova, M., Marcerou, J.-P., Nguyen, H. T., and Destrade, C., 1991, *J. Phys. II*, **1,** 831.
[16] Destrade, C., Carvalho, P. S., and Nguyen, H. T., 1996, *Ferroelectrics*, **177,** 161.
[17] Cluzeau, P., 1995, PhD thesis, Universite de Bordeaux I, p. 1399.
[18] Takanishi, Y., Takezoe, H., Fukuda, A., and Watanabe, J., 1992, *Phys. Rev. B*, **45,** 7684.
[19] Crooker, P. P., 1989, *Liq. Cryst*., **5,** 751.
[20] Li, M. H., Nguyen, H. T., and Sigaud, G., 1996, *Liq. Cryst*., **20,** 361; Li, M. H., Laux, V., Nguyen, H. T., Sigaud, G., Barois, P., and Isaert, N., 1997, *Liq. Cryst*., **23,** 389.
[21] Okabe, N., Suzuki, Y., Kawamura, I., Isozaki, T., Takezoe, H., and Fukuda, A., 1992, *Jpn. J. appl. Phys*., **31,** 793.
[22] Isozaki, T., Suzuki, Y., Kawamura, I., Mori, K., Yamamoto, Y., Yamada, Y., Orihara, H., and Ishibashi, Y., 1991, *Jpn J. appl. Phys*., **30,** 1573.
[23] Hori, K., and Endo, K., 1993, *Bull. chem. Soc. Jpn*., **66,** 46.
[24] Zareba, I., Allouchi, H., Cotrait, M., Destrade, C., and Nguyen, H. T., 1996, *Acta Cryst*., **C52,** 441.
[25] Gray, G. W., 1988, *Zehn Arbeiten über Flussige Kristalle*, Kongress und Tagenungerichte der Martin-Luther-Universität, Halle-Wittenburg, Vol. 22.
[26] Demus, D., Marzotko, D., Sharma, N. K., and Wiegelben, A., 1980, *Krist. und Tech*., **15,** 331.
[27] Kutzumitzu, S., Yamade, M., and Yano, S., 1994, *Liq. Cryst*., **16,** 1109.
[28] Goodby, J. W., Dunmur, D. A., and Collings, P.J., 1995, *Liq. Cryst*., **19,** 703.
[29] Levelut, A.-M., Germain, C., Keller, P., Liebert, L., and Billard, J., 1983, *J. Phys. (Fr.)*, **44,** 623; Levelut, A.-M., Hallouin, E., Bennemann, D., Heppke, G., and Lotzsch, D., 1997, *J. Phys. II (Fr.)*, **7,** 981.
[30] Kutnjak, Z., Garland, C. W., Schatz, C. G., Collings, P. J., Booth, C. J., and Goodby, J. W., 1996, *Phys. Rev. E*, **53,** 4955.
[31] Kutnjak, Z., Garland, C. W., Passmore, J. L., and Collings, P. J., 1995, *Phys. Rev. Lett*., **74,** 4859.
[32] Singh, U., Collings, P. J., Booth, C. J., and Goodby, J. W., 1997, *J. Phys. II Fr*. **7,** 1683
[33] Lubensky, T. C., and Stark, H., 1996, *Phys. Rev. E*, **53,** 714.